atmosphere

MDPI

Article

A Diagnosis of Some Dynamical Processes Underlying a Higher-Latitude Typhoon Using the Multiscale Window Transform

Lan Wang [1] and X. San Liang [1,2,*]

1 School of Atmospheric Sciences, Nanjing University of Information Science and Technology, 219 Ningliu Blvd, Nanjing 210044, China; wanglan@nuist.edu.cn

2 School of Marine Sciences, Nanjing University of Information Science and Technology, 219 Ningliu Blvd, Nanjing 210044, China

* Correspondence: sanliang@courant.nyu.edu

Received: 1 May 2017; Accepted: 30 June 2017; Published: 3 July 2017

Abstract: The typhoon Damrey that hit Jiangsu the populous coastal province of China on 2 August 2012 is a rarely seen tropical cyclone in that it has a higher latitude origin, and it is part of a twin typhoon. In this study, a recently developed analysis tool—multiscale window transform (MWT) and the MWT-based localized multiscale energy and vorticity analysis (MS-EVA)—is applied to investigate its genesis and maintenance. The fields are reconstructed onto three scale windows: large-scale, tropical cyclone–scale, and cumulus convection–scale windows. It is found that the track of Damrey is well along the edge of the subtropical high. Its birth is mainly caused by a strong barotropic instability in the lower troposphere around 24°–25° N. Its later amplification, however, is quite different, related to a baroclinic instability in the upper troposphere. Also discovered in this study is that a strong center of upscale canonical transfer exists over the East China Sea at the mouth of Yangtze River, which accounts for the rapid decay of Damrey before landing.

Keywords: typhoon Damrey; twin typhoon; multiscale window transform; multiscale energetics; barotropic instability; baroclinic instability

1. Introduction

On 2 August 2012, a typhoon called Damrey hit Jiangsu the most densely-populated province in China, and caused a heavy damage to the region and its surrounding provinces, such as Fujian, Zhejiang, and Shandong. Damrey is unique in that it originated in a relatively high latitude and moreover it was actually part of a twin typhoon. The other part, Saola, also landed on China several hours earlier. Figure 1 shows the tracks of the two typhoons.

Damrey and Saola appeared together on the same day, 28 July, over the western Pacific Ocean. Saola formed over the ocean east of the Philippines, while Damrey formed in higher latitudes (up to 24.8° N). In early August, Damrey landed directly on Jiangsu (a rare event) and was the most powerful typhoon to ever land north of Yangtze River. In moving westward, Damrey was weaker than its twin, Saola. In the beginning, Saola moved rather quickly, but slowed down as the two cyclones got closer together. After landing, Damrey turned northward, decayed rapidly, and disappeared.

This important and interesting synoptic scale phenomenon, however, has not been well studied. To our best knowledge, there has been no report on this rare higher-latitude cyclogenesis. In this paper, we use a newly-developed methodology, namely the multiscale energy and vorticity analysis (MS-EVA), to investigate Damrey's cyclogenesis.

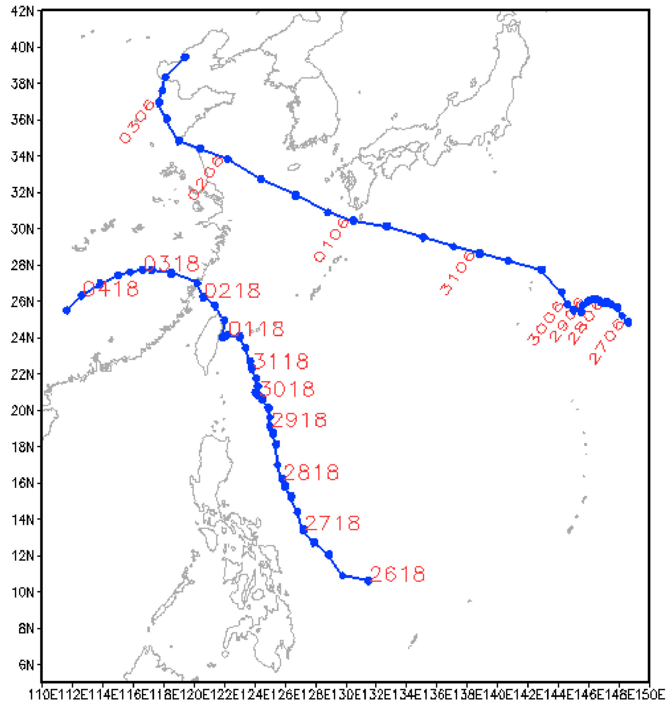

Figure 1. The tracks of Damrey (upper) and Saola (lower). Data are from China Meteorological Administration.

Tropical cyclogenesis has a close relation with multiscale interaction. For example, it has been proposed (see Chueng [1] and the references therein) that tropical cyclogenesis may be triggered by meso-scale processes under the control of large-scale systems, such as tropical upper tropospheric troughs [2–4], easterly waves [5,6], monsoon troughs [7–12], Madden-Julian oscillation (MJO) [13–16], etc. However, tropical cyclogenesis has seldom been investigated within the context of multiscale energetics; a few studies, include Ooyama [17], Papin [18], and Duan et al. [19], among others. The present study provides an investigation from this angle. Our objective is to gain some insight into typhoons that originate at higher latitudes. In this sense, Damrey may not be representative because it is one of a twin pair. However, since higher-latitude typhoons are rare, and those that cause significant loss are even rarer, we do not have many choices. At the very least, a case study of Damrey may enrich our understanding to some extent.

The following section is a brief introduction of MS-EVA, the new methodology. We first apply it to reconstruct the two cyclones (Section 3.1), then analyze the underlying dynamical processes using the MS-EVA-based instability analysis (Section 3.2). The sensitivity of the analysis results to the scale parameters is tested afterwards. This study is summarized in Section 4.

2. Data and Methodology

2.1. Data

Due to the mesoscale processes involved in tropical cyclones, we choose the ERA-interim data with a resolution of $0.125^\circ \times 0.125^\circ$. The time span is from 1 July to 2 September 2012, with an interval of 6 hours. This gives a time series of 256 steps, or 2^8 steps, as required by the analysis (see below).

2.2. Multiscale Window Transform (MWT) and Localized Multiscale Energy and Vorticity Analysis (MS-EVA)

The methodology of this study is the localized multiscale energy and vorticity analysis, or MS-EVA (cf. [20]), and the MS-EVA-based theory of finite-amplitude baroclinic and barotropic instabilities. This is a systematic line of work; a comprehensive description is beyond the scope of this paper.

The following is just a very brief introduction; for details and comparison to the traditional local energetics formalism, refer to a recent comprehensive review [20].

The MS-EVA is based on a new functional analysis tool called multiscale window transform (MWT) developed by Liang and Anderson [21]. MWT decomposes a function space into a direct sum of orthogonal subspaces, each with an exclusive range of scales. Such a subspace is termed a scale window, or simply a window. MWT was originally developed for a faithful representation of the multiscale energies on the resulting scale windows in order to make multiscale energetics analysis possible. This is a feature lacking in traditional filters, the outputs of which are fields in physical space, while multiscale energy is a concept in phase space that is connected to its physical space counterpart through the Parseval equality in functional analysis. Liang and Anderson [21] realized that, just as in the case of the Fourier transform and inverse Fourier transform, there exists a transfer-reconstruction pair for a subclass of specially devised orthogonal filters. This motivates the introduction of MWT and its counterpart, multiscale window reconstruction (MWR). MWR functions like a filter, producing decomposed fields in physical space, while MWT produces transform coefficients in phase space. MWT has many nice properties, one being the property of marginalization, which allows for a precise representation of multiscale energy (and any quadratic quantities) as the product of the MWT coefficients (up to some constant). (Note: it is NOT the product of the MWR or filtered fields!).

In this study, we will need three scale windows, namely, a large-scale window, a tropical cyclone-scale window (or simply cyclone window), and a cumulus convection-scale window (or convection window). For easy reference, they are denoted by $\varpi = 0, 1, 2$ respectively. These windows can be demarcated on the wavelet spectrum by three "window bounds": j_0, j_1, and j_2, which are the upper wavelet scale levels. In other words, given a series of scales with the time span τ, then $2^{-\mathrm{j}_0}\tau$, $2^{-\mathrm{j}_1}\tau$, and $2^{-\mathrm{j}_2}\tau$ are the upper bounds for the respective three windows.

For a given series $u(t)$, the application of the MWT yields two types of quantities: one is the MWT coefficients in phase space, $\hat{u}_\mathrm{n}^{\sim\varpi}$, and the other is the MWR in physical space, $u^{\sim\varpi}(t)$, for $\varpi = 0, 1, 2$. As mentioned above, the multiscale energy can be easily obtained. For example, the cyclonic scale energy extracted from $u(t)$ is simply $\left(\hat{u}_\mathrm{n}^{\sim 1}\right)^2$ multiplied by some constant. (Again, one cannot write it as $\left(u^{\sim 1}\right)^2$! This is the very difficulty with the classical filters which cannot have energy represented.) Since $\hat{u}_\mathrm{n}^{\sim\varpi}$ is localized, with location labelled by n in time domain, this essentially solves the oddity between localization and multiscale decomposition.

Take MWT on both sides of the primitive equations and we obtain the localized multiscale energetics. One issue remains, that is, the distinguishment of transfer and transport processes from the intertwined nonlinear terms, which is very important for this study, since it is directly related to the cyclogenesis processes. For a scalar field u within a flow $\mathbf{v}$, the transfer from the large-scale window to the cyclone window proves [20] to be,

$$\Gamma_\mathrm{n}^1 = -E_\mathrm{n}^1 \nabla \cdot \mathbf{v}_u^1, \text{where } \mathbf{v}_u^1 = \frac{(\widehat{\mathbf{v}u})_\mathrm{n}^{\sim 1}}{\hat{u}_\mathrm{n}^{\sim 1}} \tag{1}$$

and E_n^1 is the cyclone energy at time step n. For arbitrary scale window $\varpi(\varpi = 0, 1, 2)$, the transfer may be written as,

$$\Gamma_\mathrm{n}^\varpi = \frac{1}{2}\left[(\widehat{\mathbf{v}u})_\mathrm{n}^{\sim\varpi} \cdot \nabla \hat{u}_\mathrm{n}^{\sim\varpi} - \hat{u}_\mathrm{n}^{\sim\varpi} \nabla \cdot (\widehat{\mathbf{v}u})_\mathrm{n}^{\sim\varpi}\right] \tag{2}$$

which is in a Lie bracket form, just as the Poisson bracket in Hamiltonian mechanics. This transfer possesses a very interesting property, namely,

$$\sum_\varpi \sum_\mathrm{n} \Gamma_\mathrm{n}^\varpi = 0 \tag{3}$$

as proved in [20]. Physically this means that the transfer is a mere redistribution of energy among the scale windows, without generating or destroying energy as a whole. This property, though simple to state, does not hold in the classical Reynolds-decomposition based energetic formalisms. To distinguish it from those one may have encountered in the literature, the above transfer is termed "canonical transfer."

With theory, the multiscale kinetic energy (K) and available potential energy (A) equations now can be obtained for a geophysical fluid system. The details are referred to [20]. Here, we just symbolically write them as,

$$\dot{K}^{\varpi} = -\nabla \cdot \mathbf{Q}_K^{\varpi} - \nabla \cdot \mathbf{Q}_P^{\varpi} + \Gamma_K^{\varpi} - b^{\varpi} + F_K^{\varpi}, \tag{4}$$

$$\dot{A}^{\varpi} = -\nabla \cdot \mathbf{Q}_A^{\varpi} + \Gamma_A^{\varpi} + b^{\varpi} + F_A^{\varpi} + S_A^{\varpi}, \tag{5}$$

where the $-\nabla \cdot \mathbf{Q}_E (E = K, A)$ terms denote the multiscale transport processes on a specified scale window, and the Γ terms are the canonical transfers among different windows. In the equations, the location index n has been suppressed for clarity. Other notations are summarized in Table 1. Note that all the terms are localized both in space and in time; in other words, they are all four-dimensional field variables, distinguished notably from the classical formalisms in which localization is lost in at least one dimension of space or time to achieve the scale decomposition. Processes intermittent in space and time are thus naturally embedded in Equations (4) and (5). A schematic of the flowchart is shown in Figure 2.

Table 1. Symbols for the multiscale energetic terms. (The location index n is suppressed for clarity; $\varpi = 0, 1, 2$ denotes the large-scale window, tropical cyclone window, and cumulus convection window, respectively).

Kinetic Energy (KE)		Available Potential Energy (APE)	
$\dot{K}^{\varpi}$	Time rate of change of KE	$\dot{A}^{\varpi}$	Time rate of change of APE
$\mathbf{Q}_K^{\varpi}$	Flux of KE	$\mathbf{Q}_A^{\varpi}$	Flux of APE
Γ_K^{ϖ}	Canonical KE transfer	Γ_A^{ϖ}	Canonical APE transfer
$-b^{\varpi}$	Rate of buoyancy conversion	b^{ϖ}	Rate of inverse buoyancy conversion
$\mathbf{Q}_P^{\varpi}$	Pressure flux	S_A^{ϖ}	Source/Sink (usually negligible)
F_K^{ϖ}	Dissipation	F_A^{ϖ}	Diffusion

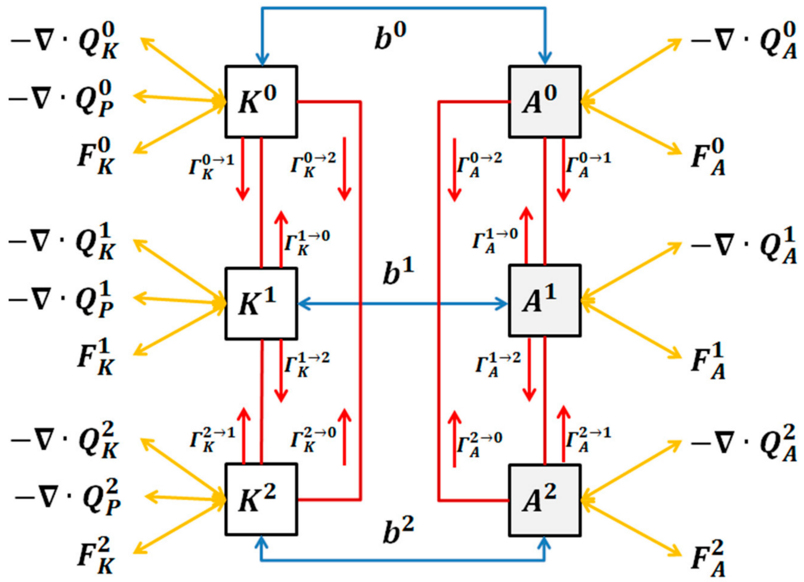

Figure 2. Multiscale energy pathway for a three-window decomposition (denoted as 0, 1, and 2, respectively). The red arrows represent the canonical energy transfers, and the blue arrows for the buoyancy conversions.

In Equations (4) and (5), the canonical transfer terms are Γ_K^1 and Γ_A^1, which mean, respectively, the KE and APE transferred to window 1 or the cyclone window from other windows, including windows 0, 2, and even the cyclone window itself. An interaction analysis can help to select out these transfers of different origins; see [20] for details. Here we simply use the superscripts $0 \to 1$, $2 \to 1$, among others, to indicate the transfer from window 0 to window 1 and that from window 2 to window 1, respectively. In [22], it has been rigorously established that these transfers correspond precisely to the two important geophysical fluid flow processes, i.e., the barotropic instability and baroclinic instability. If we consider windows 0 and 1 (respectively large-scale and cyclone-scale), then $\Gamma_K^{0\to1} > 0$ means that the cyclone-scale window receives kinetic energy from the large-scale flow, and the system is through a barotropic instability process. In a similar way, $\Gamma_A^{0\to1} > 0$ corresponds to a baroclinic instability process where the cyclone-scale window receives available potential energy from the large-scale window. Conversely, if $\Gamma_K^{0\to1}/\Gamma_A^{0\to1}$ is zero or negative, the system is then barotropically/baroclinically stable. This canonical transfer-based instability theory agrees with, but is a localized generalization of, the classical, globally defined instability theory (e.g., Pedlosky [23]). For this reason, in the following we will also refer to these two terms as barotropic and baroclinic transfers.

If the windows considered are 1 and 2, the above instability theory still holds. The entailing instabilities are now referred to as secondary barotropic and baroclinic instabilities. Again, it should be mentioned that these are rigorously established results which are generically applicable in both atmospheric and oceanic circulations. For details, see the original derivations by Liang and Robinson [22].

3. Result

3.1. General Circulation Analyses

3.1.1. MS-EVA Setup

Although the duration of a tropical cyclone is generally three to eight days, its life cycle from birth as tropical turbulence at the cumulus convection scale to final decay may last over 10 days. Here, we try two different time scale levels—3 (corresponding to 16 d) and 2 (32 d)—as the lower bound for the tropical cyclone. The upper bound j_1 is chosen to be 7. Turbulences on scales less than a day are regarded as cumulus convective disturbances. Comparing the reconstruction results, we find that the lower bound of $j_0 = 2$ gives the best cyclone separation. We hence use only the case $j_0 = 2$. The parameters for MS-EVA are summarized in Table 2.

Table 2. Multiscale energy and vorticity analysis (MS-EVA) parameters.

Parameter	Value
Window bounds (j_0, j_1, j_2)	2, 7, 8 (64 d, 32 d, 1 d)
Horizontal Grid	801 × 561
Vertical Levels	975 hPa, 950 hPa, 925 hPa, 900 hPa, 875 hPa, 850 hPa, 825 hPa, 800 hPa, 750 hPa, 700 hPa, 650 hPa, 600 hPa, 550 hPa, 500 hPa, 450 hPa, 400 hPa, 350 hPa, 300 hPa, 250 hPa, 225 hPa, 200 hPa, 175 hPa, 150 hPa, 125 hPa, 100 hPa, 70 hPa, 50 hPa, 30 hPa, 20 hPa, 10 hPa
Spatial Resolution	0.125°
Time Interval	6 h

3.1.2. Circulation Analysis

We chose the following pressure levels to analyze the circulation: 975 hPa, 850 hPa, 700 hPa, 500 hPa and 300 hPa. They respectively represent the boundary layer, the top of the boundary layer, lower, middle and upper troposphere. Figure 3 shows the geopotential field (left) and that reconstructed on the large-scale window (right).

According to previous studies [24,25], from late July to early August, in the middle and high latitudes at 500 hPa, the atmosphere over eastern Asia is controlled by the westerly flow in the south of a broad low, while a ridge occupies aloft over the Seas of Okhotsk and Japan. In lower latitudes, the subtropical high lies further northward. These features are seen in the left panels of Figure 3. As shown there, the circulation takes a form with lows to the west and a high to the east at 975 hPa. Low pressure covers lands with intensity decreasing with height. The high pressure over the ocean is the subtropical high with a northwestern ridge around 30° N. Both tropical cyclones, Damrey and Saola are clear through the levels up to 300 hPa. Damrey forms at the edge of the subtropical high and moves westwards along its southern boundary. Saola appears over the ocean to the east of the Philippines, a little bit far away from subtropical high. It moves toward the northwest.

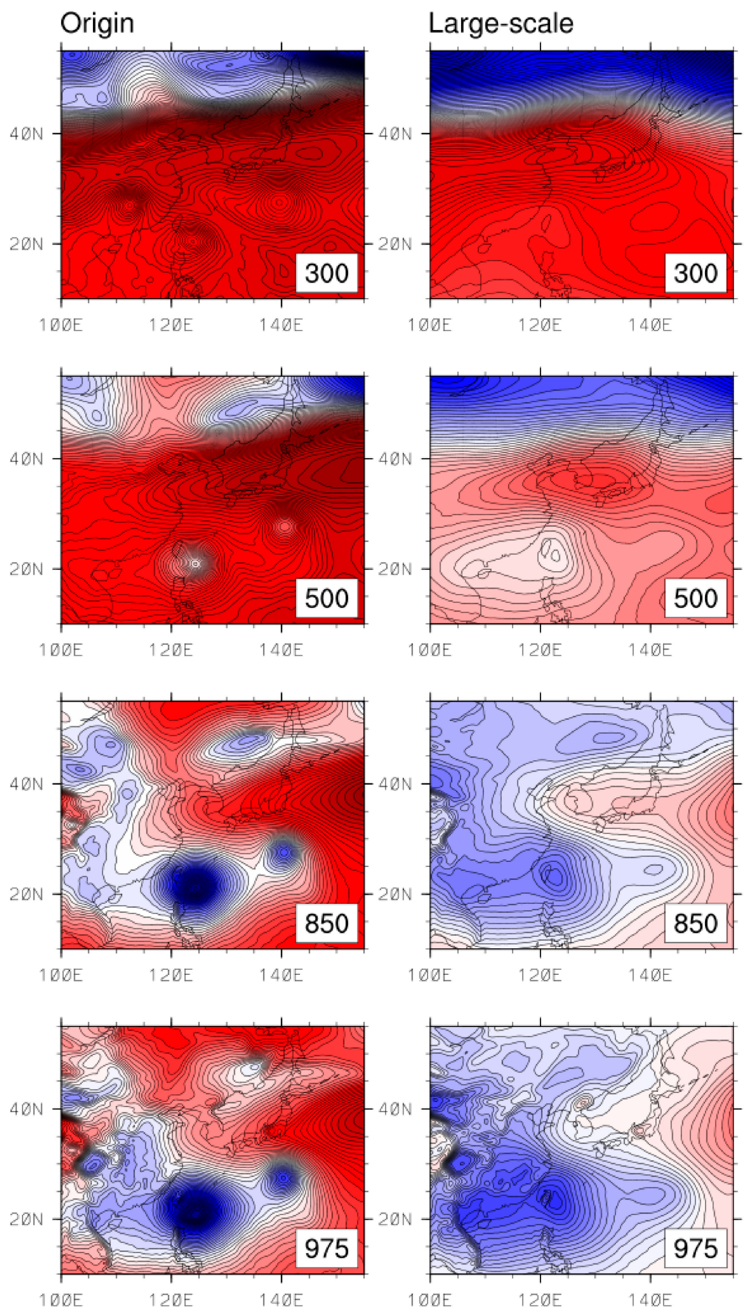

Figure 3. The original geopotential ($m^2 \cdot s^{-2}$; **left**) and its reconstruction on the large-scale window ($m^2 \cdot s^{-2}$; **right**) on 30 July, 2012, at 975 hPa, 850 hPa, 500 hPa, and 300 hPa.

To better visualize the circulation, we use the MWT to separate the cyclones out of the original fields. The fields, geopotential in particular, are reconstructed on three scale windows—large-scale window, tropical cyclone–scale window (or cyclone scale), and cumulus convection–scale window (or simply convection scale).

On the large scale window (right in Figure 3), at 975 hPa, the general feature of the geopotential is low in the west and a high in the east. Compared to the original field, the interface between the high and low pressures here is more strictly along the land boundary in middle and high latitudes. Another noteworthy feature is an eastward protuberance of low pressure over the West Pacific Warm Pool (WPWP) with the center over Taiwan. As for the high pressure, its center is located above the ocean at 30° N–37° N, east of 150° E. These results in a large-scale geopotential field with a pattern shown in the right-bottom panel of Figure 3. In the lower troposphere, the large-scale geopotential pattern to the south of 40° N is similar to that in the boundary layer (975–850 hPa). The intensity of the low pressure is slightly reduced. A new high center appears over the region covering the south of the Sea of Japan, and it is intensified with height. To the north of 40° N, the region is nearly all covered by low pressure. Upward into the middle and upper troposphere, there is a high pressure band between 25° N–35° N. The analysis above suggests that the subtropical high is narrow, lying farther in the north throughout the troposphere with a deep zonal easterly as its southern boundary. This explains why Damrey moved westward in higher latitudes.

From above, we see a large-scale boundary-layer geopotential pattern with lows in the west and a high in the east, the interface of which is slightly different from that in the original field. We know that the surface will have a stronger impact on the atmosphere in low levels, and a warm surface tends to cause a shallow warm low. In summer, both the warm land and the WPWP form the warm surface. The WPWP and the land together influence the form of the pressure. Obviously, the pattern in Figure 3 looks more like the climate state of the atmosphere in low levels in summer, which is disguised in the original field. The geopotential pattern in the boundary layer varies with height. The low weakens with height, but the high gets strengthened slightly. Since the formation of the low pressure is influenced significantly by the surface, the weakening is within expectation. On the other hand, the subtropical high results from the downdraft branch of the Hadley circulation so the increasing distance from the surface does not have much impact on its intensity. This gives rise to a pattern with a low in the north and a high in the south above 700 hPa, which becomes more obvious as height increases. Besides, we find a clear structure of the south Asian high at 150 hPa (no shown); its center moves from the ocean to the Tibetan Plateau.

On the cyclone window are the tropical cyclones, especially Damrey. Figure 4 shows the cyclone scale geopotential field (shading) superimposed on the large scale field (black solid line). It is easy to find that the cyclones both formed at the interface of the low and high pressure, while Saola was born far from the interface in the original field. After formation, the weaker Damrey moved westward along the edge, while the stronger Saola moved northwestward to the low over Taiwan. The two eventually hit China in the north and south, respectively. After that, Saola rapidly weakened and moved southwestward along the interface; this is indiscernible in the original field.

Take the instance when the closed isopleths appear as the birth time of a tropical cyclone. At 975 hPa and 850 hPa, Damrey is formed on 27 July at 0:00, while Saola is formed earlier, before 26 July. At 700 hPa and 500 hPa, the closed isopleths of Damrey appear slightly later than at lower levels (6:00, 27 July). At 300 hPa, there exists a broad low over the formation region, quite different from the lower levels. Even though the discreteness of time and the interval of contours result in inaccuracy in finding Damrey's birth time, the relative sequence of appearance of closed isopleths suggests that both Damrey and Saola were born first in lower levels.

The cyclones last over a week. At 975 hPa, Damrey's closed isopleths completely disappear on 4 August at 12:00. At 850 hPa, 700 hPa and 500 hPa, Damrey dies on 3 August at 12:00 or earlier. That is to say, Damrey first forms but last dies in lower levels.

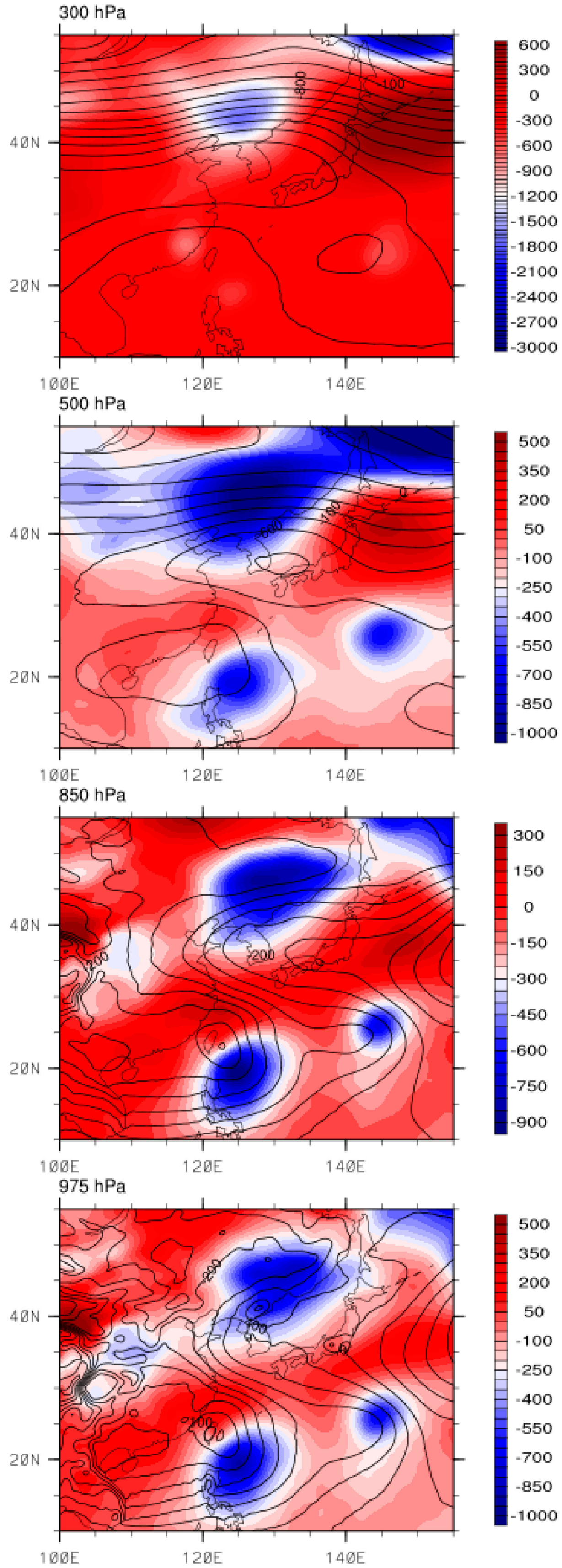

Figure 4. Geopotential anomaly ($m^2 \cdot s^{-2}$) on the cyclone window (shading) on 30 July 2012, at 975 hPa, 850 hPa, 500 hPa, and 300 hPa. Contoured is the large-scale field.

3.2. Multiscale Energy Transfer Analyses

We now look at the dynamical processes underlying Damrey using the MS-EVA methodology. We will focus on the canonical energy transfers among the three scale windows as they are the keys to the formation of vortices. For convenience, we divide the life cycle into three stages: formation, intensification, and decay. The formation stage of Damrey is taken from its birth time to 0:00, 31 July; after that, Damrey undergoes its intensification and decay stages. We chose 30 July and 2 August as the representative times for the presentation of the results on the formation and intensification stages, respectively. Though the resulting multiscale energetics are varying in time, their patterns respectively for each stage are similar.

3.2.1. Formation Stage

In the formation stage, Damrey evolves from a tropical depression to a tropical storm at 0:00 28 July. It is then strengthened continuously. By 31 July, it becomes a strong tropical storm.

Kinetic Energy Transfer

Figure 5 shows the KE transfer between the large-scale window and cyclone window. Below 300 hPa, in the formation regions of both tropical cyclones it is positive ($\Gamma_K^{0\to1} > 0$); that is to say, the system is barotropically unstable. But at 300 hPa, it is stable locally.

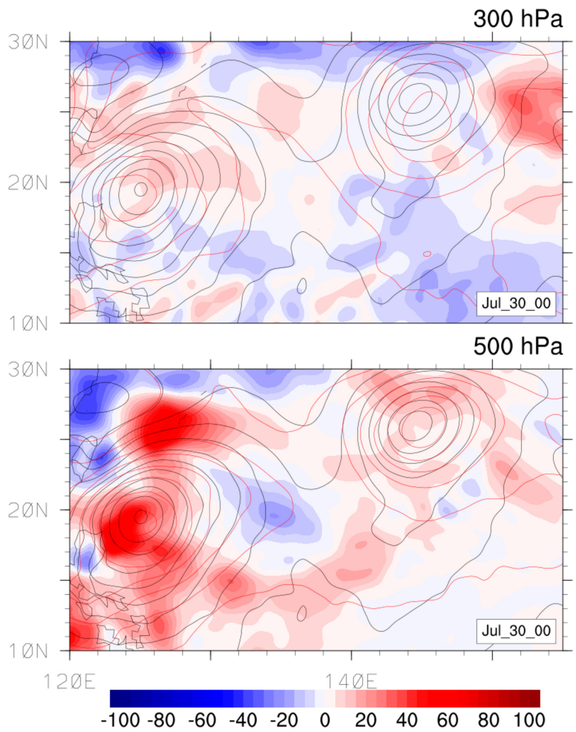

Figure 5. Canonical kinetic energy (KE) transfers ($10^{-5}\cdot m^2\cdot s^{-3}$) between large-scale window and cyclone window on 30 July 2012, at 500 hPa and 300 hPa. Shaded are KE transfers between the large-scale window and cyclone window, where a positive value stands for a KE transfer from the large-scale window to the cyclone window. The red contour lines are the geopotential on the cyclone window at the corresponding levels. Also superimposed on the maps are the cyclone-scale geopotential at 975 hPa (in black).

The KE transfer between convection and cyclone windows during the formation stage is shown in Figure 6, which becomes significant from 30 July. Around the Damrey, the system undergoes a weak secondary stability ($-\Gamma_K^{1\to2} > 0$) in the middle troposphere and a weak secondary barotropic instability ($-\Gamma_K^{1\to 2} < 0$) in the upper troposphere. Generally, these transfers are rather weak compared to that between the large-scale and cyclone scale windows.

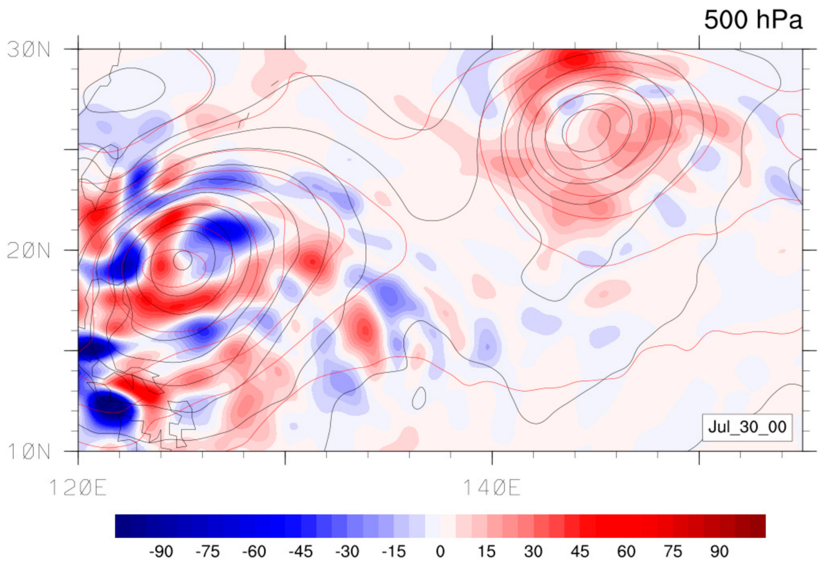

Figure 6. Same as Figure 5, but for KE transfer ($10^{-5}\cdot m^2\cdot s^{-3}$) between the convection window and cyclone window on 30 July 2012, at 500 hPa.

Available Potential Energy Transfer

The APE transfer between large-scale and cyclone windows at low levels (975 hPa, 850 hPa and 700 hPa) is insignificant except above Taiwan (no shown). Considering that the data around Taiwan under 700 hPa are invalid (the highest altitude of Taiwan's terrain is 3997m), we may safely say that the APE transfer is not important at low levels. Above 500 hPa (Figure 7), we can find clear transfers in the formation region. Especially at 300 hPa, there is a baroclinic instability band between 15° N–25° N. However, this band does not cover the region which Damrey moves through, except a protuberance at 147° E, 25° N.

The behaviors of the two tropical cyclones look similar. At the beginning of the formation of Saola, the system overhead is baroclinically stable at 300 hPa. As it moves northwestward, it enters a baroclinically unstable area aloft and then more and more closed contours appear on the geopotential field, even though the atmosphere at 500 hPa is locally stable. It then slows down and intensifies rapidly. The rapid intensification region corresponds to the maximal baroclinic instability. As for Damrey, it also forms under a baroclinically stable atmosphere at 300 hPa, but is baroclinically unstable at 500 hPa, and then moves westward. It gets intensified first in lower layers beneath that protuberance of the baroclinical instability band from 28 July. Both tropical cyclones form at a baroclinically stable region at 300 hPa but experience a rapid growth in a baroclinically unstable environment.

The APE transfer between the cyclone and convection windows is rather weak and is not shown here.

From the discussion above, we see that Damrey gets KE from the background in middle and lower layers (lower than 500 hPa) and loses KE to the large-scale window and the convection window in upper troposphere. This is in according with the Bottom-Up hypothesis proposed by Zhang and Bao [26], who argued that deep convection will develop under the organization of mesoscale convective vortices (MCV) and activate the development from bottom to top, and finally lead to the formation of tropical cyclones. This also explains why Damrey formed from lower to higher levels.

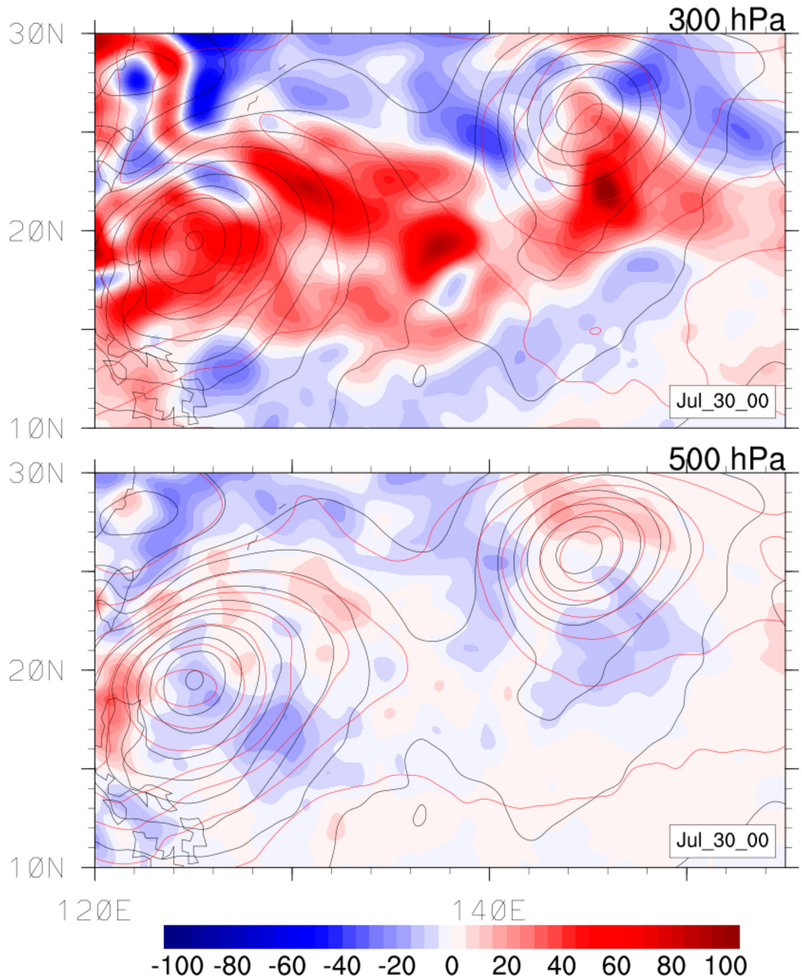

Figure 7. Same as Figure 5, but for canonical APE transfers ($10^{-5} \cdot m^2 \cdot s^{-3}$) on 30 July 2012, at 500 hPa and 300 hPa.

On the other hand, Damrey at first gets APE from the large-scale window in middle levels (500 hPa), which is returned to the same window at 300 hPa. On the whole, the net APE transfer between the large-scale and cyclone windows is insignificant. This suggests that the formation of Damrey is not caused by accumulating of APE. However, the later intensification of the tropical depression is closely related to baroclinic processes. Besides, the transfer between convection and cyclone windows is always small. That is to say, cumulus convections do not serve as an energy source, partly agreeing with the idea about energy source of tropical cyclone in air-sea interaction theory proposed by Emanuel [27–29], who regards the function of cumulus convections in tropical cyclone formation as transporting energy rather than providing energy. However, his proposal that the energy source be moisture entropy (estimated by equivalent potential temperature in his papers) from the underlying ocean is not verified here. Instead, Damrey formed in a way of barotropic instability, with the energy source being the background field.

3.2.2. Intensification and Decay

After 31 July, Damrey experiences another intensification. After 12:00 1 August, it goes into a stage of rapid development. However, until 6:00, 2 August, Damrey starts to decay, though it has not landed yet.

Kinetic Energy Transfer

From Figure 8, after the cyclones leave their formation regions, the KE transfer between the large-scale and cyclone windows takes a pattern of inverse cascade (barotropic stability) in the north and barotropic instability in the south. From 975 hPa (no shown) to 500 hPa, the barotropic stability is weak except a conspicuous region of inverse cascade lies in the East China Sea near the mouth of Yangtze River. At 300 hPa, there is a wide inverse cascade region, north of 30° N. On the track of Damrey, the troposphere is barotropically stable. Damrey reaches the mouth of Yangtze River on 2 August at 6:00, when it stops growing. Barotropic transfer appears unfavourable to the maintenance of Damrey.

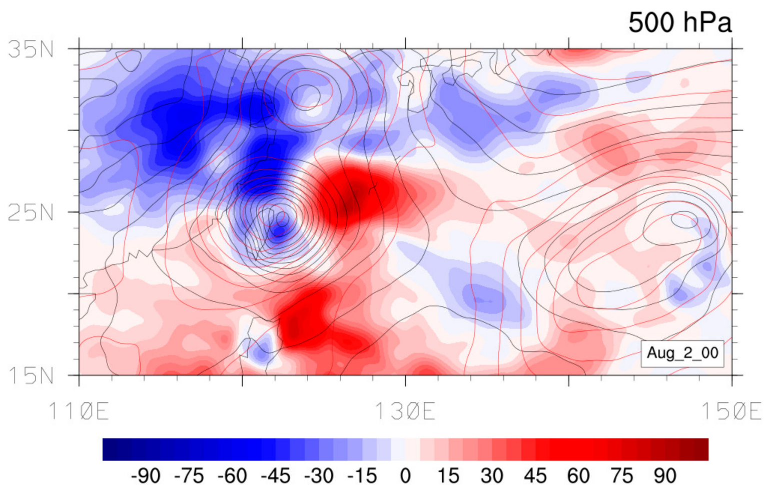

Figure 8. Same as Figure 5, but on 2 August 2012, at 500 hPa.

For the KE transfers between convection and cyclone windows (Figure 9), they mainly exist in the surroundings of the cyclones. Their intensity is positively related to the strength of the cyclones. Besides, surrounding the tropical cyclone, secondary instabilities and stabilities lie alternatively. Here, it is hard to say whether convection scale serves as energy source or sink to the cyclone.

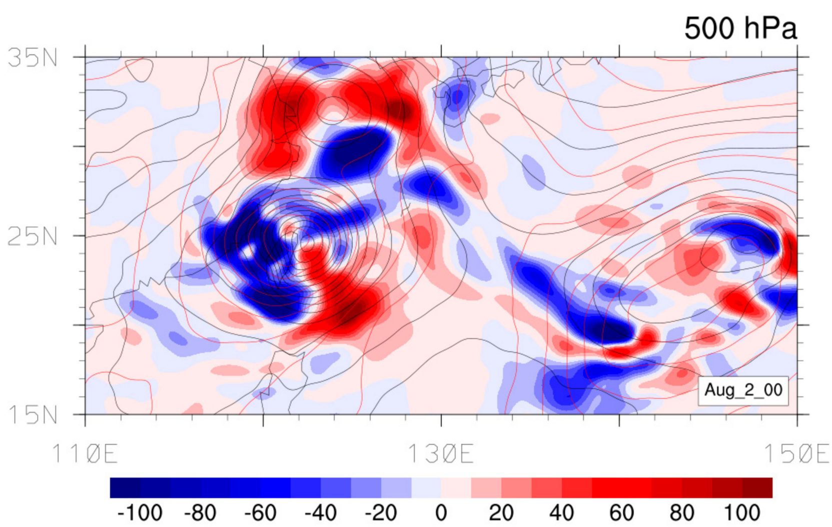

Figure 9. Same as Figure 6, but on 2 August 2012 at 500 hPa.

Available Potential Energy Transfer

The APE transfers are shown in Figure 10. It is interesting to note that, at 850 hPa (not shown) in the area east of China, the atmosphere is baroclinically stable, while a baroclinic instability takes place in the coastal region between 25° N–30° N. The intensity of the APE transfer becomes weaker with height until 500 hPa. At 300 hPa over the land, the system is largely baroclinically unstable, although the local atmosphere over the sea, to the east of Yangtze River's estuary and to the south of Japan is still dominated by an inverse cascade. It seems that the APE transfer is not favorable to the maintenance of Damrey in upper troposphere before it reaches the mouth of Yangtze River where the whole troposphere is baroclinically stable.

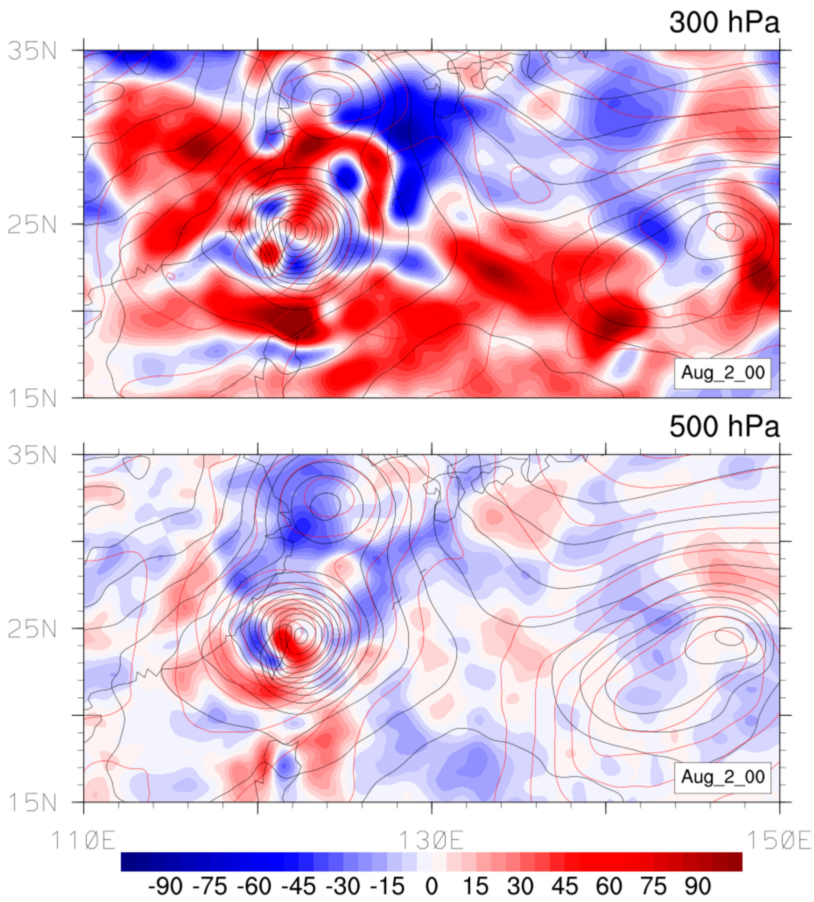

Figure 10. Same as Figure 7 but at 500 hPa and 300 hPa on 2 August 2012.

For the APE transfer between the convection and cyclone windows, it is rather small in the levels below 500 hPa, but at 300 hPa there exists a secondary upscale transfer ($-\Gamma_A^{1\to 2} < 0$). For Damrey, the transfer is weaker (no shown).

To summarize, even though the canonical energy transfers between large-scale and cyclone windows are unfavorable to the maintenance of Damrey in upper troposphere, only the intense KE and APE inverse cascade over the estuary of Yangtze River throughout the troposphere lead to the quick decay of Damrey before its landing. The energy transfers between the convection and cyclone windows are mainly around the cyclones and their intensity is correlated to that of the cyclones.

3.3. Sensitivity Study

The above analysis is with the window bounds $j_0 = 2$ and $j_1 = 7$, which correspond to a time scale of 32 d and 1 d. To see whether it is sensitive to the choice of these parameters, we have tested with the combinations as shown in Table 3. Here, Case 1 is the standard run. Other choices have also been considered but are physically irrelevant. For example, the lower bound of eight days does not make sense, since this event lasted more than 10 days; on the other hand, a lower bound of 64 d is far beyond typhoon scale. These considerations end up with the above combinations.

Table 3. Sensitivity tests for the choice of parameters of MS-EVA.

Case	j_1	j_0	Remark
Case 1	7 (1 day)	2 (32 days)	Standard Run
Case 2	6 (2 days)	2 (32 days)	
Case 3	7 (1 day)	3 (16 days)	
Case 4	6 (2 days)	3 (16 days)	

The final result of Case 2 (no shown) is essentially the same as Case 1, which has been presented above. For Case 3, the pattern is similar, though some differences exist. Figure 11a shows the 500-hPa geopotenial reconstructed on the cyclone-scale window. Compared to Figure 4, the resulting structures are almost the same. The canonical transfers have also been compared. On the canonical KE and APE transfer maps, the distributions (Figure 11b,c) are similar to the 500-hPa transfers respectively in Figures 5 and 7, except that the APE transfer is stronger here. The result of Case 4 is similar to Case 3. We may then safely conclude that the multiscale energetics are not sensitive to the choice of window bounds, provided that the bounds are within a reasonable range.

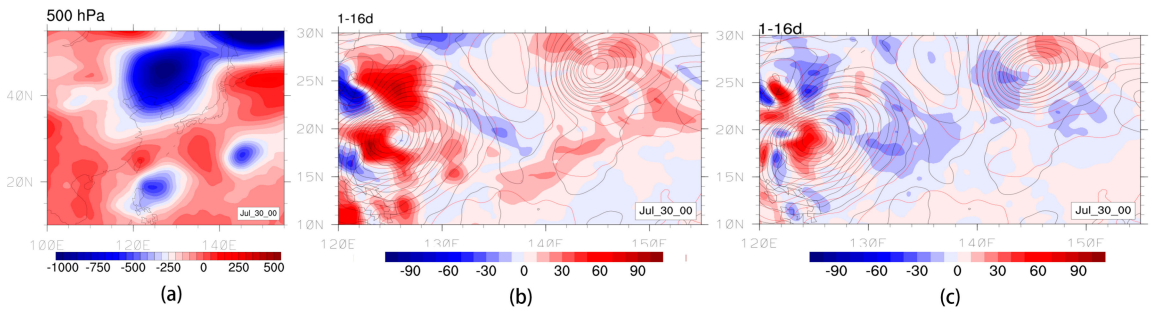

Figure 11. MS-EVA analysis with window bounds (1 d, 16 d). (**a**) Cyclone-scale reconstruction of geopotential, (**b**) cyclone-scale canonical KE transfer, and (**c**) APE transfer at 500 hPa on 30 July 2012.

4. Conclusions and Discussion

The twin typhoons, Damrey and Saola, during late July–early August, 2012, were a special phenomenon. The higher latitude genesis of Damrey made it a rare tropical cyclone that directly landed on Jiangsu Province. Under the influences of the two tropical cyclones, during those days, East China suffered serious flooding and other disasters.

In this study, we investigated the energetics that lead to the formation, intensification, and decay of the phenomena using a newly developed methodology: multiscale window transfer (MWT) and localized multiscale energy and vorticity analysis (MS-EVA). Based on the diagnostic results, the two cyclones formed due to some barotropic instabilities in the lower layer. In the region of 145° E–150° E, 20° N–25° N, a significant barotropic instability area has been identified, corresponding to the birthplace of the initial disturbance of Damrey. This explains why Damrey formed in so high a latitude. The initial disturbance obtained kinetic energy from the large-scale background in lower layers, and developed upward. Duan and Wu [19] drew a similar conclusion that the barotropic transfers make significant contributions to tropical cyclogeneses that take place at the confluence region of and inside the monsoon trough. This is also supported by the results of Maloney [15], which state that during the formation stage of tropical cyclones, eddy kinetic energy is largely transferred from that of large-scale circulation. Formation of the cyclone has little relation to baroclinic processes, but the development is indeed related to baroclinic instability in the upper troposphere. Both tropical cyclones' rapid intensifications after formation happened at the strong baroclinic instability areas in the upper troposphere. Damrey, in particular, was strengthened right at a spot of baroclinic instability, though within a baroclinically stable system.

After formation, the energy transfers between the large-scale and cyclone windows are rather unfavorable to the maintenance of Damrey in the upper troposphere, while Saola was still in a favorable environment. This partially explains why Saola was more strengthened than Damrey. The intense barotropic and baroclinic inverse cascades over the East China Sea at the mouth of Yangtze River are responsible for the rapid decay of Damrey before landing. However, Damrey was close to Saola then. As Fujiwhara [30,31] and Guinn and Schuber [32] showed, two vortices will interact with each other in the course of approaching, and the strong one tends to merge the weak one. The final decay of Damrey was likely related to the interaction with Saola through this mechanism. Besides, other processes, such as upper-trough and land-sea interaction, may also be important.

We want to emphasize that the results here are just from a case study. Damrey is not typical of higher-latitude typhoons due to the presence of Saola, and hence the resulting multiscale processes may not be typical, either. Nonetheless, that different mechanisms account for the formation and development of an event has also been discovered with other atmospheric phenomena such as atmospheric blocking [33] and stratospheric sudden warming [34]. We will keep checking this in future studies.

Acknowledgments: We are grateful to two anonymous reviewers for their constructive suggestions. ECMWF and CMA are appreciated for making the data available. Lan Wang thanks Yuanbing Zhao, Yang Yang, and Jiwang Ma for their valuable advice and discussions. This study was supported by the State Oceanic Administration through the National Program on Global and Air-Sea Interaction (GASI-IPOVAI-06), by the National Science Foundation of China (NSFC) under Grant 41276032, and by the Jiangsu Provincial Government through the Jiangsu Chair Professorship and the 2015 Jiangsu Program for Entrepreneurship and Innovation Group.

Author Contributions: X. San Liang: idea, methodology (mathematics and programing), analysis, and result interpretation, writing; Lan Wang: computation, data analysis, result interpretation, writing.

Conflicts of Interest: The authors declare no conflict of interest. The founding sponsors had no role in the design of the study; in the collection, analyses, or interpretation of data; in the writing of the manuscript, and in the decision to publish the results.

References

1. Cheung, K.K.W. Large-scale environmental parameters associated with tropical cyclone formations in the western North Pacific. *J. Clim.* **2010**, *17*, 466–484. [CrossRef]
2. Mcbride, J.L.; Keenan, T.D. Climatology of tropical cyclone genesis in the Australian region. *Inter. J. Clim.* **1982**, *2*, 13–33. [CrossRef]
3. Montgomery, M.T.; Farrell, B.F. Tropical cyclone formation. *J. Atmos. Sci.* **1993**, *50*, 285–308. [CrossRef]
4. Sadler, J.C. A role of the tropical upper tropospheric trough in early season typhoon development. *Mon. Weather Rev.* **1974**, *104*, 57. [CrossRef]
5. Landsea, C.W. A climatology of intense (or major) Atlantic hurricanes. *Mon. Weather Rev.* **1993**, *121*, 1703. [CrossRef]
6. Molinari, J.; Vollaro, D.; Skubis, S.; Dickinson, M. Origins and mechanisms of eastern Pacific tropical cyclogenesis: A case study. *Mon. Weather Rev.* **2010**, *128*, 2000. [CrossRef]
7. Gray, W.M. Global view of the origin of tropical disturbances and storms. *Mon. Weather Rev.* **1968**, *96*, 87. [CrossRef]
8. Ritchie, E.A.; Holland, G.J. Large-scale patterns associated with tropical cyclogenesis in the western Pacific. *Mon. Weather Rev.* **1999**, *127*, 2027–2043. [CrossRef]
9. Qiu, W.Y.; Wu, L.G. Influence of north-west Pacific monsoon depression on tropical cyclogenesis. *J. Meteorol. Sci.* **2015**, *35*, 237–247. (In Chinese)
10. Li, X.Y.; Wu, L.G.; Zong, H.J. Analysis of influence of monsoon gyres on tropical cyclogenesis over the western North Pacific. *Trans. Atmos. Sci.* **2014**, *37*, 653–664. (In Chinese)

11. Zong, H.J.; Wu, L.G. Re-examination of tropical cyclone formation in monsoon troughs over the western North Pacific. *Adv. Atmos. Sci.* **2015**, *32*, 924–934. [CrossRef]
12. Zhang, W.L.; Zhang, D.L.; Wang, A.S.; Cui, X.P. An investigation of the genesis of typhoon Durian (2001) from a monsoon trough. *Acta Meteorol. Sin.* **2008**, *67*, 811–827. (In Chinese)
13. Zhu, C.W.; Nakazawa, T.; Li, J.P. Modulation of tropical depression/cyclone over the Indian-Western Pacific oceans by Madden-Julian oscillation. *J. Meteorol. Sci.* **2004**, *62*, 42–50. (In Chinese)
14. Maloney, E.D.; Hartmann, D.L. Modulation of hurricane activity in the gulf of Mexico by the Madden-Julian oscillation. *Science* **2000**, *287*, 2002–2004. [CrossRef] [PubMed]
15. Maloney, E.D.; Hartmann, D.L. The Madden-Julian oscillation, barotropic dynamics, and North Pacific tropical cyclone formation. Part I: Observations. *J. Atmos. Sci.* **2001**, *58*, 2545–2558. [CrossRef]
16. Sun, Z.; Mao, J.Y.; Wu, G.X. Influences of intraseasonal oscillations on the clustering of tropical cyclone activities over the western North Pacific during boreal summer. *J. Meteorol. Sci.* **2009**, *33*, 950–958. (In Chinese)
17. Ooyama, K.V. Conceptual evolution of the theory and modeling of the tropical cyclone. *J. Meteorol. Soc. Jpn. Ser. II* **1982**, *60*, 369–380. [CrossRef]
18. Papin, P. Using the Rossby radius of deformation as a forecasting tool for tropical cyclogenesis. In Proceedings of the National Conference on Undergraduate Research, Ithaca, NY, USA, 31 March–2 April 2011.
19. Duan, J.J.; Wu, L.G. Kinetic energy budget analysis of tropical cyclogenesis precursors in the monsoon trough. *J. Meteorol. Sci.* **2016**, *36*, 141–148. (In Chinese)
20. Liang, X.S. Canonical transfer and multiscale energetics for primitive and quasi-geostrophic atmospheres. *J. Atmos. Sci.* **2016**, *73*. [CrossRef]
21. Liang, X.S.; Anderson, D.G.M. Multiscale window transform. *Siam J. Multiscale Model. Simul.* **2007**, *6*, 437–467. [CrossRef]
22. Liang, X.S.; Robinson, A.R. Localized multi-scale energy and vorticity analysis: II. Finite-amplitude instability theory and validation. *Dyn. Atmos. Oceans* **2007**, *44*, 51–76. [CrossRef]
23. Pedlosky, J. *Geophysical Fluid Dynamics*, 2nd ed.; Springer: New York, NY, USA, 1987; 710p.
24. Tao, Y.W. Analysis of the August 2012 atmospheric circulation and weather. *Meteorol. Mon.* **2012**, *28*, 1429–1435. (In Chinese)
25. Zhou, N.F. Analysis of the July 2012 atmospheric circulation and weather. *Meteorol. Mon.* **2012**, *38*, 1307–1312. (In Chinese)
26. Zhang, D.L.; Bao, N. Oceanic cyclogenesis as induced by a mesoscale convective system moving offshore. Part ii: Genesis and thermodynamic transformation. *Mon. Weather Rev.* **1996**, *124*, 2206. [CrossRef]
27. Emanuel, K.A. An air-sea interaction theory for tropical cyclones. Part I: Steady-state maintenance. *J. Atmos. Sci.* **1986**, *43*, 585–605. [CrossRef]
28. Emanuel, K.A. The theory of hurricanes. *Ann. Rev. Fluid Mech.* **2003**, *23*, 179–196. [CrossRef]
29. Rotunno, R.; Emanuel, K.A. An air–sea interaction theory for tropical cyclones. Part II: Evolutionary study using a nonhydrostatic axisymmetric numerical model. *J. Atmos. Sci.* **1987**, *44*, 542–561. [CrossRef]
30. Fujiwhara, S. On the growth and decay of vortical systems. *Q. J. R. Meteorol. Soc.* **1923**, *49*, 75–104. [CrossRef]
31. Fujiwhara, S. The natural tendency towards symmetry of motion and its application as a principle in meteorology. *Q. J. R. Meteorol. Soc.* **1921**, *47*, 287–292. [CrossRef]
32. Guinn, T.A.; Schubert, W.H. Hurricane spiral bands. *J. Atmos. Sci.* **1993**, *50*, 3380. [CrossRef]
33. Ma, J.W.; Liang, X.S. Dynamical processes underlying the wintertime Atlantic blockings. *J. Atmos. Sci.* **2017**, in press.
34. Xu, F.; Liang, X.S. On the generation and maintenance of the 2012–2013 sudden stratospheric warming. *J. Atmos. Sci.* **2017**, in press.